International Journal of Heat and Mass Transfer 82 (2015) 460–467

Contents lists available at ScienceDirect

International Journal of Heat and Mass Transfer

journal homepage: www.elsevier.com/locate/ijhmt

Unsteady thermal boundary layer flows of a Bingham fluid in a porous medium

D. Andrew S. Rees [a,*], Andrew P. Bassom [b]

[a] Department of Mechanical Engineering, University of Bath, Bath BA2 7AY, UK
[b] School of Mathematics and Statistics, The University of Western Australia, Crawley, WA 6009, Australia

ARTICLE INFO

Article history:
Received 9 July 2014
Received in revised form 20 October 2014
Accepted 20 October 2014
Available online 28 November 2014

Keywords:
Porous media
Boundary layer
Unsteady flow
Convection
Bingham fluid
Yield stress

ABSTRACT

In this paper we consider some unsteady free convection flows of a Bingham fluid when it saturates a porous medium. These flows are induced by suddenly raising the constant temperature of a vertical bounding surface from that of the uniform ambient value to a new constant level. As time progresses heat conducts inwards and this induces flow. We consider both a semi-infinite domain and a vertical channel of finite width. Of interest here are (i) how the presence of yield surfaces alters the classical results for Newtonian flows and (ii) the manner in which the locations of the yield surfaces change as time progresses.

1. Introduction

Bingham fluids are fluids with a yield stress but which are otherwise Newtonian, i.e. they have a linear stress–strain relationship once the yield stress is exceeded. These fluids arise in a variety of natural and industrial settings including the oil industry, agriculture and the food processing industry; see for example works by Barnes [1], Jeong [2], Maßmeyer [3], Shenoy [4] and Sochi and Blunt [5]. Other commonly-studied yield-stress fluids are Casson fluids and Herschel–Bulkley fluids, and both of these have a nonlinear stress/strain relationship post-yield.

There currently exists a fairly small body of work which considers the convection of a Bingham fluid. Many of these are concerned with convection in sidewall-heated cavities which, for a Newtonian fluid, admit flow at all nonzero values of the Rayleigh. When the cavity is filled with a Bingham fluid, flow is not possible until the Rayleigh number is sufficiently large that buoyancy forces are able to overcome the yield stress. In such contexts the critical Rayleigh number appears to be a multiple of a convective Bingham number. More detailed information may be gleaned from the papers by Hassan et al. [6], Turan et al. [7–9], Vikhansky [10] and Vola et al. [11].

More directly relevant to the present paper are the analyses of Yang and Yeh [12] and Bayazitoglu et al. [13] who studied free convection in a sidewall-heated channel. Once more, convection arises whenever the Rayleigh number is sufficiently large, but the velocity profile is characterised by having two plugs of unyielded fluid placed symmetrically about the centreline of the channel and moving in opposite directions — Karimfazli and Frigaard [14] refer to this as a five-region flow because each plug is surrounded by yielding fluid thereby giving five regions which alternate between yielding and not yielding. The studies contained in [12,13] have been extended in different directions. For example, Patel and Ingham [15] also applied a driving pressure gradient and they describe the transition from the five-region natural convection velocity profile to the more familiar three-region Poiseuille profile where the unyielded plug is in the centre of the channel. Barletta and Magyari [16] consider free convection, but one of the boundaries moves parallel with itself, a Couette flow. The free convective five-region velocity profile also undergoes a transition to a three-region profile as the velocity of the boundary increases, but now the two plugs are attached to the boundaries with yielding fluid in-between. Karimfazli and Frigaard [14] also consider free convection, but the temperatures of the bounding surfaces increase linearly with distance whilst maintaining a constant local difference. They present a complicated scenario whereby the number of regions within the velocity profile increases as the convective Bingham number decreases towards zero; the caveat is that this happens

* Corresponding author.
E-mail addresses: D.A.S.Rees@bath.ac.uk (D. Andrew S. Rees), andrew.bassom@uwa.edu.au (A.P. Bassom).

http://dx.doi.org/10.1016/j.ijheatmasstransfer.2014.10.047
0017-9310/

Nomenclature

Latin letters

$\mathcal{D}$	equal to $\ln\delta$
$F(\mathrm{Rb})$	location of the yield surface
g	gravity
G	threshold body force
K	permeability
L	length scale
p	pressure
p_x	pressure gradient in the x-direction
Q	total vertical velocity flux
Ra	Darcy–Rayleigh number
Rb	Rees–Bingham number
t	time
T	temperature (dimensional)
T_0	ambient (cold) temperature
T_1	temperature of heated surface
u	vertical Darcy velocity
x	vertical coordinate
y	horizontal coordinate
z	dummy variable

Greek letters

α	thermal diffusivity
β	coefficient of cubical expansion
δ	defined in terms of Rb in Eq. (27)
η	similarity variation
η_y	location of yield surface
θ	temperature (nondimensional)
μ	dynamic viscosity
ρ	reference density
σ	heat capacity ratio

Other symbols

$-$	dimensional quantities

only when the stratification parameter is above 7.8532, otherwise a five-region flow which is similar to that of Yang and Yeh [12] is obtained in the small convective Bingham number limit.

It is also important to mention the unsteady analysis of Kleppe and Marner [17] who consider the boundary layer flow induced by a semi-infinite uniformly hot surface; this is the Bingham-fluid analogue of the Newtonian free convective boundary layer problem that was solved by Ostrach [18]. Using an unsteady solver written for a Cartesian coordinate system, they determined the evolution with time of an impulsive change in the temperature of the bounding surface, and eventually obtained steady solutions of a one-plug, three-region type.

While undertaking the preliminary literature review for the chapter by Rees [19], which is concerned with the state-of-the-art for convection of a Bingham fluid in a porous medium, the very large number of papers which exists on yield stress fluids in general includes only a relatively very small handful on convection in porous media and all of these are on boundary layer flows. Perhaps the reason for such a void in the literature is a lack of obvious applications for the convection of a Bingham fluid in porous media, but, as is always true for yield-stress fluids, there are numerical difficulties associated with determining where the yield surface is and perhaps this has deterred research on the topic.

The present paper is part of the beginning of an effort to fill that void by considering an unsteady free convection problem. We will consider the effect on a cold saturated porous medium of raising suddenly the temperature of a vertical bounding surface to a new constant level. Unlike the paper of Kleppe and Marner [17] the present idealised configuration does not have a leading edge, which means that the temperature and velocity field may be described using a non-similar analysis, and boths fields are independent of the vertical coordinate. Heat gradually diffuses from the hot surface thereby introducing buoyancy forces, and if these forces are sufficiently large then flow will arise. In this type of problem the induced flow field may be found analytically, and it is possible to determine the locations of the yield surfaces numerically using a simple Newton–Raphson scheme. Two cases are considered, namely convection in a semi-infinite domain and convection in a channel of finite and constant thickness.

2. Governing equations

One of the earliest papers to consider the flow of a Bingham fluid in a porous medium is that of Pascal [20]. He presented a threshold gradient model based on experimental observations which is the very simplest possible model that may be used. In one dimension and for isothermal flow it may be written in the form,

$$\overline{u} = \begin{cases} -\dfrac{K}{\mu}\left[1 - \dfrac{G}{|\overline{p}_{\overline{x}}|}\right]\overline{p}_{\overline{x}} & \text{when } |\overline{p}_{\overline{x}}| > G, \\ 0 & \text{otherwise}, \end{cases} \tag{1}$$

where we use G to denote the threshold gradient (or threshold body force) above which the fluid yields. We see that the fluid velocity increases linearly with the pressure gradient, $\overline{p}_{\overline{x}}$, once the threshold is exceeded. A commonly used but more complicated alternative is the Buckingham–Reiner model (see [21–23]) which is given by,

$$\overline{u} = \begin{cases} -\dfrac{K}{\mu}\left[1 - \dfrac{4}{3}\left(\dfrac{G}{|\overline{p}_{\overline{x}}|}\right) + \dfrac{1}{3}\left(\dfrac{G}{|\overline{p}_{\overline{x}}|}\right)^4\right]\overline{p}_{\overline{x}} & \text{when } |\overline{p}_{\overline{x}}| > G, \\ 0 & \text{otherwise}. \end{cases} \tag{2}$$

It may be shown easily that the fluid velocity rises quadratically at first once the threshold gradient is exceeded but this eventually relaxes to a linear variation. In the present paper we will confine our attention to the threshold model.

Once buoyancy is introduced as an extra body force, the threshold model given in Eq. (1) becomes,

$$\overline{u} = \begin{cases} -\dfrac{K}{\mu}\left[1 - \dfrac{G}{|\overline{p}_{\overline{x}} - \rho g\beta(T - T_0)|}\right](\overline{p}_{\overline{x}} - \rho g\beta(T - T_0)) & \text{when } |\overline{p}_{\overline{x}} - \rho g\beta(T - T_0)| > G, \\ 0 & \text{otherwise}. \end{cases} \tag{3}$$

Here we have assumed that the Boussinesq approximation applies when writing down the buoyancy term, and T_0 is the initial temperature of the porous medium. It is to be noted that we have also assumed that the threshold gradient, G, is independent of temperature, and this is equivalent to having a temperature-independent yield stress in the fluid. Exceptions to this situation include heavy oils [24] where the fluid becomes Newtonian above the so-called converting temperature.

In the above equations we have taken $\overline{x}$ to be the vertical coordinate and $\overline{u}$ to be the Darcy velocity in the same direction. In this idealised problem there will be no horizontal velocity, and therefore $\overline{v} = 0$. (If $\overline{v}$ had been nonzero then it would be necessary to alter the yield criterion in Eq. (3) to obtain a pair of momentum equations which are frame-invariant; see [19].) Therefore we may allow $\overline{u}$ to be a function only of the horizontal coordinate, $\overline{y}$,

and time, $\bar{t}$, and so the equation of continuity is satisfied. The final equation is that for the heat transport,

$$\sigma T_{\bar{t}} + \bar{u}T_{\bar{x}} + \bar{v}T_{\bar{y}} = \alpha\left(T_{\bar{x}\bar{x}} + T_{\bar{y}\bar{y}}\right). \tag{4}$$

Here σ is heat capacity ratio between the porous medium and the saturating fluid, and α is the thermal diffusivity of the porous medium. We may also allow T to be a function solely of $\bar{y}$ and $\bar{t}$, and therefore Eq. (4) reduces to,

$$\sigma T_{\bar{t}} = \alpha T_{\bar{y}\bar{y}}. \tag{5}$$

The governing equations, namely Eqs. (3) and (5), may be non-dimensionalised using the following scalings,

$$(\bar{x},\bar{y}) = L(x,y), \quad \bar{u} = \frac{\alpha}{L}u, \quad \bar{p} = \frac{\alpha\mu}{K}p,$$
$$T = T_0 + (T_1 - T_0)\theta, \quad \bar{t} = \frac{\sigma L^2}{\alpha}t, \quad G = \frac{\alpha\mu}{KL}\mathrm{Rb}, \tag{6}$$

where T_1 is the temperature of the hot surface, and we obtain,

$$u = \begin{cases} \mathrm{Ra}\,\theta - p_x - \mathrm{Rb}, & \mathrm{Rb} < \mathrm{Ra}\,\theta - p_x, \\ 0, & -\mathrm{Rb} < \mathrm{Ra}\,\theta - p_x < \mathrm{Rb}, \\ \mathrm{Ra}\,\theta - p_x + \mathrm{Rb}, & \mathrm{Ra}\,\theta - p_x < -\mathrm{Rb} \end{cases} \tag{7}$$

and

$$\theta_t = \theta_{yy}. \tag{8}$$

In the above the Darcy–Rayleigh number is given by

$$\mathrm{Ra} = \frac{\rho g\beta(T_1 - T_0)KL}{\mu\alpha}, \tag{9}$$

and the parameter,

$$\mathrm{Rb} = \frac{KL}{\mu\alpha}G. \tag{10}$$

This latter parameter appeared for the first time in [19] and it is clearly a scaled version of the yield pressure gradient, G. Given the presence of K and α, it may be more properly termed a porous convective Bingham number. However, there is already a Bingham number which is used in other contexts, and therefore (10) will be referred to hereinafter as the Rees–Bingham number.

A lengthscale, L, was introduced in Eq. (6) without comment. When we consider convection in a channel later, L may be taken to be the dimensional width of that channel, but in the semi-infinite domain there is no natural physical lengthscale that may be used. However, as the Darcy–Rayleigh number also includes L, one may set $\mathrm{Ra} = 1$ to give

$$L = \frac{\mu\alpha}{\rho g\beta(T_1 - T_0)K}, \tag{11}$$

as a lengthscale based upon the fluid and porous medium properties. This type of analytical device has been used in other studies [25,26]. The other possible alternative would be to use $L = \sqrt{K}$, but this yields a length corresponding to the pore or particle scale. Thus we will use the value of L given in Eq. (11) for the semi-infinite domain, and take L to be the width of the channel for the channel problem.

The initial condition in nondimensional form is simply that $\theta = 0$ at $t = 0$. For both cases we have $\theta = 1$ at $y = 0$, while we have $\theta \to 0$ as $y \to \infty$ for the infinite domain, and $\theta = 0$ at $y = 1$ for the vertical channel.

3. The semi-infinite domain

We consider first the free convective motion which is set up by suddenly raising the temperature of a vertical bounding surface from a nondimensional value of zero to $\theta = 1$. As has already been discussed we are setting $\mathrm{Ra} = 1$ in this case.

The solution of Eq. (8) for θ is well-known and may be found either by using Laplace transforms, or else by means of a self-similar analysis. It takes the form,

$$\theta = \mathrm{erfc}\,\eta = \frac{2}{\sqrt{\pi}}\int_\eta^\infty \mathrm{e}^{-\xi^2}\,\mathrm{d}\xi, \tag{12}$$

where $\eta = y/2\sqrt{t}$.

In an infinite domain we expect the suddenly-heated surface to provide only upward movement of the fluid, and therefore we may set $p_x = 0$. This means that the hydrostatic component of the vertical pressure gradient corresponds precisely to that for the ambient fluid at $\theta = 0$. When the fluid near the boundary is heated up, the buoyancy force then induces only upward motion. Therefore Eq. (7) simplifies to,

$$u = \begin{cases} \theta - \mathrm{Rb} & \text{when } \mathrm{Rb} < \theta \\ 0 & \text{when } \theta < \mathrm{Rb}. \end{cases} \tag{13}$$

Clearly, one implication of this is that flow is induced only when $\mathrm{Rb} < 1$. For larger values of Rb the buoyancy force is insufficient to cause the fluid to yield.

The total velocity flux may now be determined as a function of both Rb and time. If we define η_y (where the subscript, y, denotes yield) to be where the yield surface is, then η_y satisfies

$$\mathrm{erfc}\,\eta_y = \mathrm{Rb}. \tag{14}$$

The variation of η_y with $\log_{10}\mathrm{Rb}$ is shown in Fig. 1. The Figure confirms that flow arises only when $\mathrm{Rb} < 1$ since the region below the curve is that where the fluid moves, while the region above corresponds to a stagnant medium. It is of interest to note how slowly the yield surface varies as Rb decreases; even when $\mathrm{Rb} = 10^{-10}$ the yield surface is at $\eta_y = 4.5728$ although it has also to be said that, at such large values of η, the value of $\mathrm{erfc}\,\eta$ is super-exponentially small. If one were to use the approximation,

$$\mathrm{erfc}\,(z) \sim \frac{e^{-z^2}}{\sqrt{\pi}z} \quad (z \gg 1), \tag{15}$$

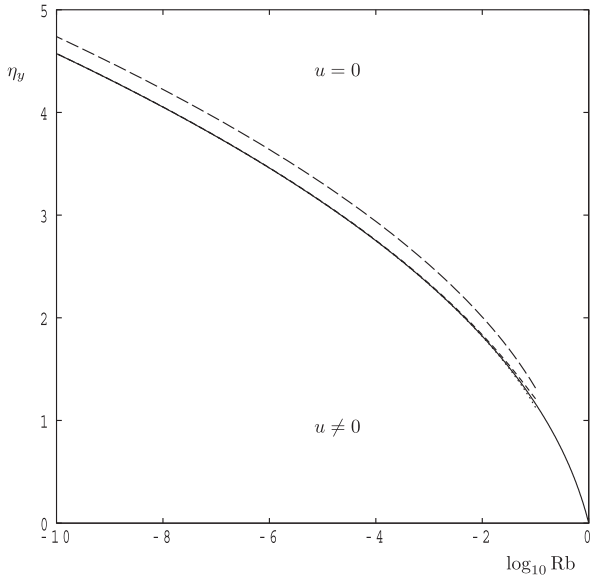

Fig. 1. The location, η_y, of the yield surface as a function of $\log_{10}\mathrm{Rb}$ (continuous line). Also shown are one term (long dashes), two terms (short dashes) and three terms (dotted) of the asymptotic series given in (29).

then it is possible to determine the following leading order expression for η_y

$$\eta_y \sim \sqrt{-\ln(\sqrt{\pi}\,\mathrm{Rb})} \tag{16}$$

for small values of Rb, and this explains the very slow increase in η_y as $\mathrm{Rb} \to 0$. A much more precise expression for η_y in terms of Rb is given in Appendix A.

Having found the value of η_y in terms of Rb, the variation with Rb of the fluid flux is now given by

$$Q = \int_0^\infty u\,dy = 2\sqrt{t}\int_0^{\eta_y} (\mathrm{erfc}\,\xi - \mathrm{Rb})\,d\xi = \frac{2\sqrt{t}}{\sqrt{\pi}}(1 - e^{-\eta_y^2}) \equiv \frac{2\sqrt{t}}{\sqrt{\pi}}F(\mathrm{Rb}). \tag{17}$$

The variation of $F(\mathrm{Rb})$ with Rb is given in Fig. 2, for reference, and we see how this scaled fluid flux decreases towards zero as $\mathrm{Rb} \to 1$, as expected. The small-Rb behaviour of $F(\mathrm{Rb})$ is also given in Appendix A.

These Figures confirm that free convective boundary layer flow is possible for the suddenly-heated problem in an infinite domain provided that $\mathrm{Rb} < 1$ or, equivalently that the threshold body force satisfies the relation,

$$G < \rho g \beta (T_1 - T_0). \tag{18}$$

We note that this criterion is independent of L, and we see that the maximum threshold body force is determined solely by the strength of the buoyancy forces.

4. The vertical channel

We begin with Eqs. (7) and (8). The cavity is assumed to be very tall but of finite height. Apart from turning regions at the top and the bottom of the cavity, the flow, when it arises, will be parallel and will be dependent only on y and t. Thus there will be no mean flow up the cavity at any time. We may also allow the domain to have unit width; this simply means that we have used the dimensional width as the lengthscale, L, and therefore the Darcy–Rayleigh number appears as a parameter.

We consider the situation where $\theta = 1$ on $y = 0$ and $\theta = 0$ on $y = 1$, with the initial condition, $\theta = 0$. The solution of (12) is found quite easily using a Laplace transform in time; we find that,

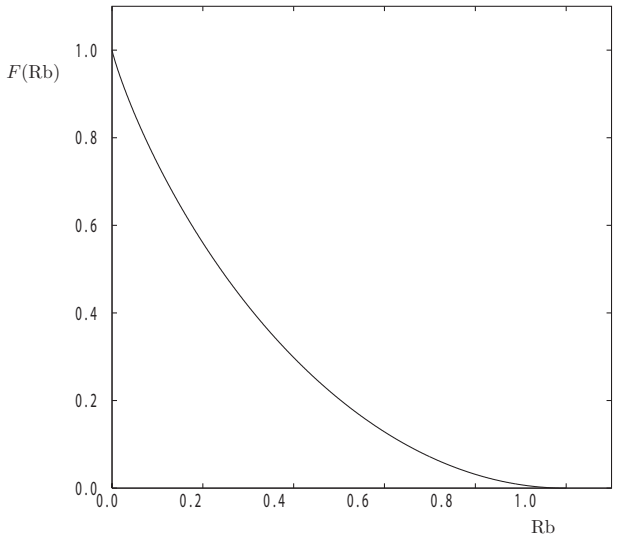

Fig. 2. The function $F(\mathrm{Rb})$ as given by Eq. (17).

$$\theta = \sum_{n=0}^{\infty}\left[\mathrm{erfc}\left(\eta + \frac{n}{\sqrt{t}}\right) - \mathrm{erfc}\left(\frac{n+1}{\sqrt{t}} - \eta\right)\right]. \tag{19}$$

Some temperature profiles at selected times are shown in Fig. 3 which shows the transition from an isolated complementary error function solution at early times towards the final simple linear profile.

As mentioned above, the fact that flow will take place within a finite cavity, albeit one which is tall, means that the upward flow which is induced by the heated surface must be balanced by an opposing downward flow near the colder vertical surface. This overall zero net upward fluid flux cannot be sustained by allowing p_x to be zero for all time, as is the case for the infinite domain. Thus the value of p_x must vary in time in order to maintain the zero-vertical-flux condition. But the circulation which is induced must also be characterised by having a central unyielded region. Working in terms of η, we may say that the two yield surfaces may be located at η_1 and η_2 where $\eta_1 < \eta_2$, and these values are given by,

$$\mathrm{Ra}\,\theta(\eta_1, t) = p_x + \mathrm{Rb}, \tag{20}$$

$$\mathrm{Ra}\,\theta(\eta_2, t) = p_x - \mathrm{Rb}; \tag{21}$$

see Eq. (7). The zero mean vertical fluid flux condition may be imposed by first defining $\eta_3 = 1/(2\sqrt{t})$ (which is equivalent to $y = 1$), we therefore need $Q = 0$ where,

$$Q = \mathrm{Ra}^{-1}\int_0^{\eta_3} u\,d\eta = \int_0^{\eta_1}\left[\theta - \frac{p_x}{\mathrm{Ra}} - \frac{\mathrm{Rb}}{\mathrm{Ra}}\right]d\eta + \int_{\eta_2}^{\eta_3}\left[\theta - \frac{p_x}{\mathrm{Ra}} + \frac{\mathrm{Rb}}{\mathrm{Ra}}\right]d\eta. \tag{22}$$

The integrations may be performed analytically and therefore we obtain,

$$\begin{aligned} Q = {} & \frac{p_x}{\mathrm{Ra}}(-\eta_1 + \eta_2 - \eta_3) + \frac{\mathrm{Rb}}{\mathrm{Ra}}(-\eta_1 - \eta_2 + \eta_3) \\ & + \frac{1}{\sqrt{\pi}}\sum_{n=0}^{\infty}\left[e^{-[\eta_0 + n/\sqrt{t}]^2} + e^{-[(n+1)/\sqrt{t} - \eta_0]^2} - e^{-[\eta_1 + n/\sqrt{t}]^2} + e^{-[(n+1)/\sqrt{t} - \eta_1]^2}\right] \\ & + \frac{1}{\sqrt{\pi}}\sum_{n=0}^{\infty}\left[e^{-[\eta_2 + n/\sqrt{t}]^2} + e^{-[(n+1)/\sqrt{t} - \eta_2]^2} - e^{-[\eta_3 + n/\sqrt{t}]^2} + e^{-[(n+1)/\sqrt{t} - \eta_3]^2}\right] \\ & - \sum_{n=0}^{\infty}\left[\left(\eta_0 + n/\sqrt{t}\right)\mathrm{erfc}\left(\eta_0 + n/\sqrt{t}\right) + \left((n+1)/\sqrt{t} - \eta_0\right)\mathrm{erfc}\left((n+1)/\sqrt{t} - \eta_0\right)\right] \\ & + \sum_{n=0}^{\infty}\left[\left(\eta_1 + n/\sqrt{t}\right)\mathrm{erfc}\left(\eta_1 + n/\sqrt{t}\right) + \left((n+1)/\sqrt{t} - \eta_1\right)\mathrm{erfc}\left((n+1)/\sqrt{t} - \eta_1\right)\right] \\ & - \sum_{n=0}^{\infty}\left[\left(\eta_2 + n/\sqrt{t}\right)\mathrm{erfc}\left(\eta_2 + n/\sqrt{t}\right) + \left((n+1)/\sqrt{t} - \eta_2\right)\mathrm{erfc}\left((n+1)/\sqrt{t} - \eta_2\right)\right] \\ & + \sum_{n=0}^{\infty}\left[\left(\eta_3 + n/\sqrt{t}\right)\mathrm{erfc}\left(\eta_3 + n/\sqrt{t}\right) + \left((n+1)/\sqrt{t} - \eta_3\right)\mathrm{erfc}\left((n+1)/\sqrt{t} - \eta_3\right)\right], \end{aligned} \tag{23}$$

where we use the definition, $\eta_0 = 0$, to preserve the symmetry of this formula.

The aim then is, for given values of Rb/Ra and t, to solve Eqs. (20) and (21) and $Q = 0$ simultaneously to obtain the values of p_x/Ra, η_1 and η_2, where Q is given by Eq. (23). This was undertaken by a straightforward three-dimensional Newton–Raphson scheme where numerical differentiation was used to derive the Jacobian

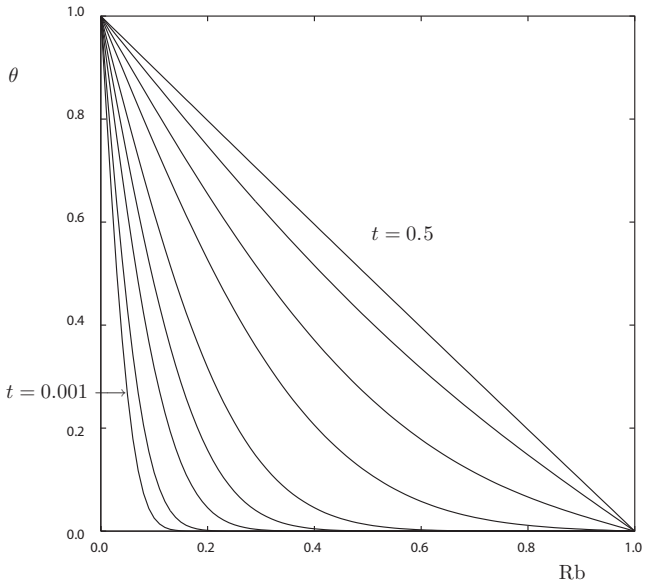

Fig. 3. Temperature profiles for the tall channel at $t = 0.001, 0.002, 0.005, 0.01, 0.02, 0.05, 0.1, 0.2$ and 0.5.

matrix. The results we present are essentially exact to machine accuracy (Fortran double precision).

The behaviour of the resulting flow in the channel may be understood with reference to Figs. 4–7. Fig. 4 shows how the positions of the yield surfaces vary in time for different values of Rb/Ra. Whenever Rb/Ra is nonzero there are always two yield surfaces. At early times the thermal boundary layer is concentrated near the hot surface, and therefore the locations of the yield surfaces move away from that surface as time progresses. At late times, the temperature profile is linear, and therefore the yield surfaces are located at equal distances either side of $y = {}^1/_2$ in all cases. In general, the width of the unyielded region is small when Rb/Ra is small, but it increases as Rb/Ra increases, finally filling the whole channel when Rb/Ra $= {}^1/_2$. Thus the presence of a right hand cold

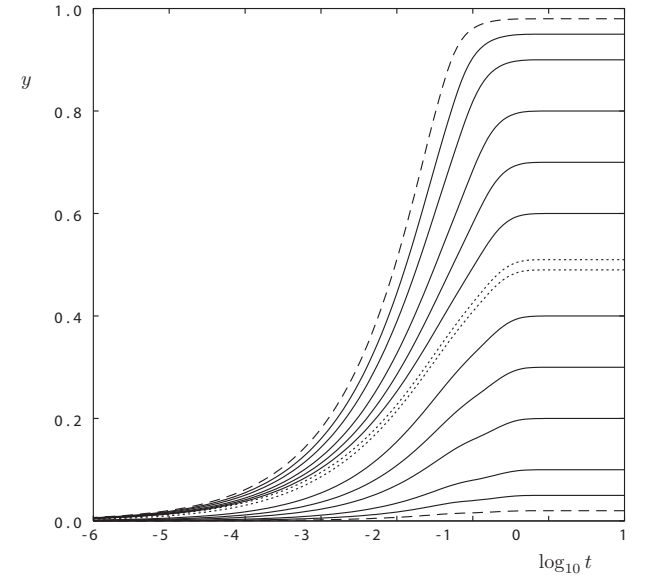

Fig. 4. Locations of the yield surfaces as functions of time for Rb/Ra = 0.01 (dotted lines), 0.1, 0.2, 0.3, 0.4, 0.45 and 0.48 (dashed lines). Each value of Rb has two yield surfaces, and the fluid is stationary between these two surfaces.

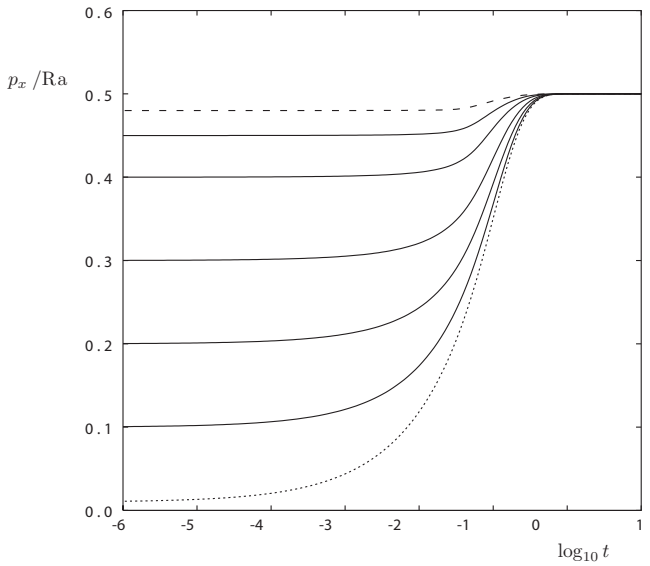

Fig. 5. Variation with time of the value of p_x/Ra; for Rb/Ra = 0.01 (dotted line), 0.1, 0.2, 0.3, 0.4, 0.45 and 0.48 (dashed line).

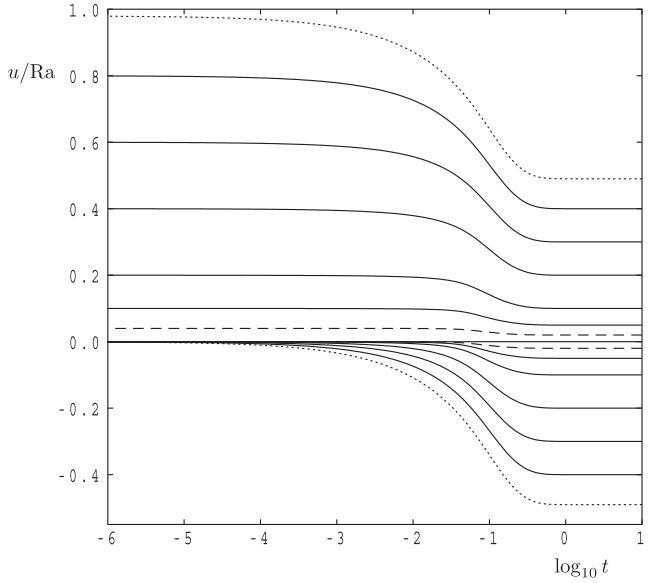

Fig. 6. Variation with time of the maximum and minimum fluid velocities for Rb/Ra = 0.01 (dotted lines), 0.1, 0.2, 0.3, 0.4, 0.45 and 0.48 (dashed lines). Curves which lie above the line, $u = 0$, represent the maxima while those below represent the minima.

boundary alters the condition for flow to arise from Rb/Ra < 1 in the case of an infinitely large domain to Rb/Ra < ${}^1/_2$ in a finite domain; in dimensional terms this is equivalent to

$$G < \frac{1}{2}\rho g\beta(T_1 - T_0). \tag{24}$$

When t is large the temperature field has reached a steady state, and we note that an overall zero fluid flux up the layer must now correspond to $p_x = \frac{1}{2}$Ra. This value of p_x may be regarded as being equivalent to changing the reference temperature in the nondimensionalisation given in Eq. (6) from T_0, the cold boundary (or ambient) temperature, to $(T_1 + T_0)/2$, which is the mean temperature of the two walls.

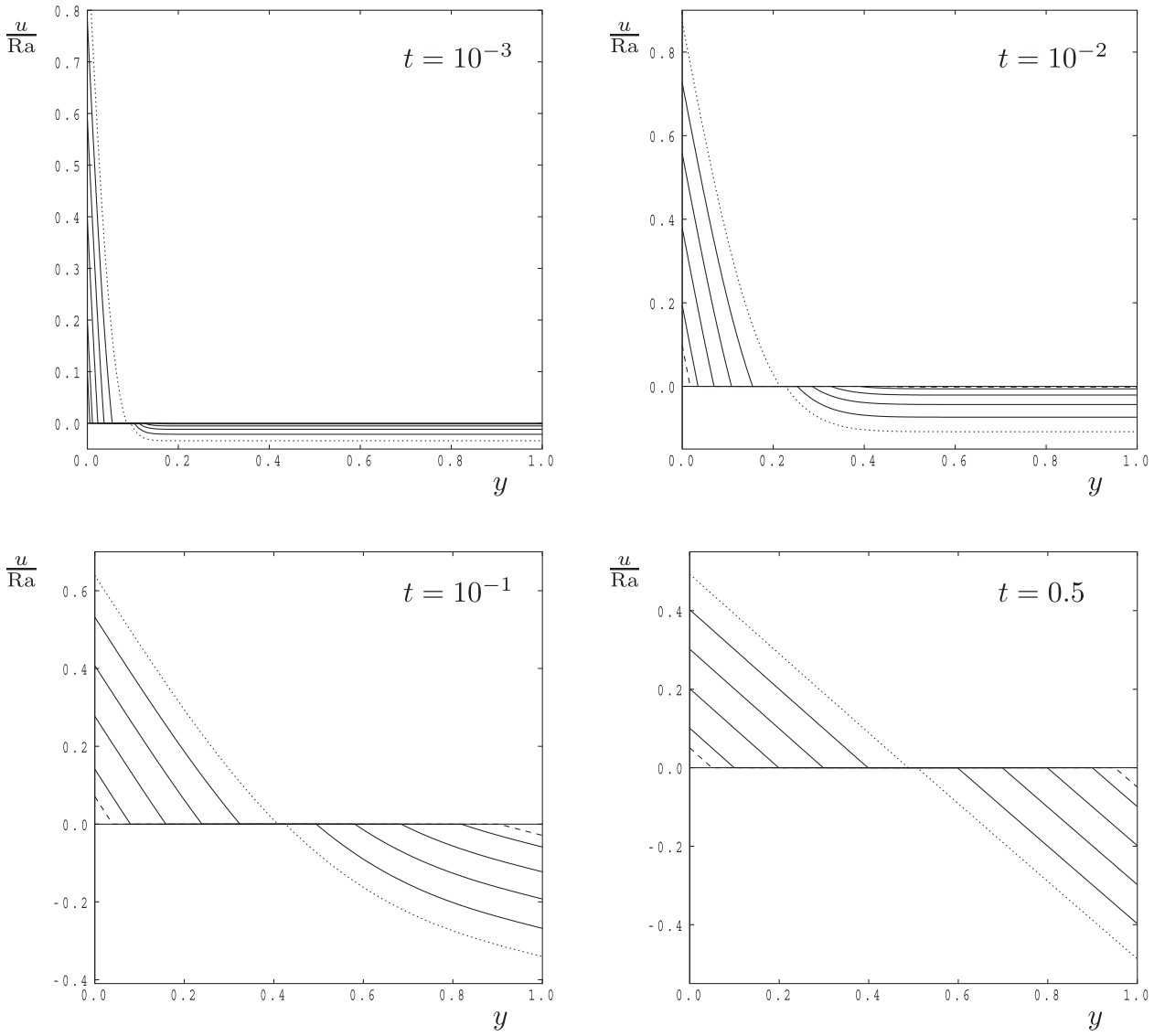

Fig. 7. Velocity profiles for Rb/Ra = 0.01 (dotted lines), 0.1, 0.2, 0.3, 0.4 and 0.45 (dashed lines). Individual frames correspond to the times indicated.

The overall variation of p_x/Ra with time is shown in Fig. 5. At early times p_x/Ra is very slightly above the value of Rb; given the form of Eq. (7) (third case), this allows for a very small but negative velocity in almost the whole cavity, and this balances a strong upward flow in the very thin thermal boundary layer near $y = 0$. Then, as time progresses, p_x adjusts towards the value, $\frac{1}{2}\mathrm{Ra}$.

Fig. 6 illustrates how the maximum and minimum vertical velocities evolve. At early times there is a strong upward flow at $y = 0$ and a very weak downward flow at $y = 1$, as mentioned above. As time progresses the system transforms into one where eventually the magnitudes of the maximum and the minimum are equal. Due to the retardation of the microscopic yield stress, the overall magnitude of the velocities at all times decreases as Rb increases. Thus when Rb is just below $\frac{1}{2}\mathrm{Ra}$ the only fluid motion arises close to the two vertical boundaries with stationary fluid occupying most of the width of the channel.

Finally, Fig. 7 shows how the induced velocity profiles depend on both Rb/Ra and t. For each choice of Rb/Ra there is range of values of y for which $u = 0$, details of which are given in Fig. 4, but they are seen explicitly here. Also seen clearly is the way in which the overall strength of the flow decreases with increasing Rb, and how the stagnant region moves towards the centre of the channel as t increases. The value, $t = 0.5$ is almost indistinguishable from the ultimate steady state and here the velocity profile is piecewise-linear.

5. Conclusions

In this paper we have considered the effect of the presence of a yield threshold on convection induced by suddenly heating a vertical surface bounding a porous medium. The temperature profile evolves in time in a manner which is independent of the fluid and, given that there is no time-derivative in the momentum equation, the flow, which arises only when the Rees–Bingham number is sufficiently small, reacts instantaneously to the changing temperature field.

We have found that convection happens in an infinite domain when the threshold gradient satisfies $G < \rho g \beta (T_1 - T_0)$ and in a finite channel when $G < \frac{1}{2}\rho g \beta (T_1 - T_0)$ — the sole reason for this difference is due to the requirement of a zero upward fluid flux for the channel. For both domains, the region of unyielded flow varies with time, and in the channel it eventually tends towards the middle of the channel. For the channel we also see that the

Table 1
Comparison of the asymptotic expansion for the location of the yield surface with the exact data given by solving (25) numerically.

$\log_{10}\epsilon$	1 Term	2 Terms	3 Terms	4 Terms	Exact
−1	1.31537833	1.21117853	1.12731613	1.20805578	1.16308715
−2	2.00818456	1.83458720	1.81773758	1.82353158	1.82138637
−3	2.51702013	2.33365336	2.32576817	2.32715218	2.32675377
−4	2.93904328	2.75563596	2.75068224	2.75118708	2.75106391
−5	3.30765181	3.12682285	3.12323560	3.12346328	3.12341327
−6	3.63911330	3.46163325	3.45881877	3.45893482	3.45891074
−7	3.94280747	3.76883333	3.76651192	3.76657563	3.76656258
−8	4.22472671	4.05418851	4.05220845	4.05224495	4.05223724
−9	4.48897548	4.32171856	4.31998897	4.32001024	4.32000538
−10	4.73851095	4.57435358	4.57281590	4.57282820	4.57282497

hydrostatic pressure gradient needs to evolve in time in order to maintain an overall zero upward flux of fluid.

Finally, we note that if we had taken the Buckingham–Reiner law (Eq. (2)) instead of the threshold law (Eq. (1)) as the governing momentum equation, then the yield surfaces presented here would be unaltered. However, there would be slight quantitative changes in how p_x varies in time and in the velocity profiles themselves where the magnitude of the velocity at any point will be reduced by a small amount. An identical comment about the position of the yield surface may be made for Casson and Herschel–Bulkley fluids, but the strength of the induced flow could alter quite substantially from what has been presented here. For example, for the Herschel–Bulkley fluid, the effective viscosity is very high immediately post-yield when it is a shear-thinning fluid, and therefore there would be a strong reduction in the resulting flow strength. The opposite conclusion applies for a shear-thickening fluid. These changes are routine to determine and are not presented here.

Conflict of interest

None declared.

Appendix A

The primary aim of this Appendix is to provide an asymptotic analysis of the small values of ϵ of the solution of

$$\operatorname{erfc}\eta = \epsilon \tag{25}$$

(i.e. Eq. (14)) where the value of η is the location of the yield surface.

It is straightforward to show that a large-η expansion for $\operatorname{erfc}\eta$ is

$$\operatorname{erfc}\eta = \frac{e^{-\eta^2}}{\eta\sqrt{\pi}}\left[1 - \frac{1}{2\eta^2} + \frac{3}{4\eta^4} + \cdots\right]. \tag{26}$$

It proves very convenient to work with δ as the small parameter instead of ϵ where δ is defined according to

$$e^{-1/\delta^2} = \epsilon\sqrt{\pi}, \quad \text{i.e.} \quad \delta = \frac{1}{\sqrt{-\ln(\epsilon\sqrt{\pi})}}. \tag{27}$$

Therefore we are solving,

$$\frac{e^{-\eta^2}}{\eta}\left[1 - \frac{1}{2\eta^2} + \frac{3}{4\eta^4} + \cdots\right] = e^{-1/\delta^2} \tag{28}$$

and it is clear that the leading order solution will be $\eta \sim \delta^{-1}$.

Subsequent terms in the series for η in terms of δ take the form of odd integral powers of δ with coefficients that are polynomials in $\mathcal{D} = \ln\delta$. By straightforward substitution and the equating of like terms, it is possible to show that,

$$\eta = \frac{1}{\delta} + \frac{\mathcal{D}}{2}\delta - \frac{\mathcal{D}^2 + 2\mathcal{D} + 2}{8}\delta^3 + \frac{\mathcal{D}^3 + 4\mathcal{D}^2 + 8\mathcal{D} + 7}{16}\delta^5 + O(\mathcal{D}^4\delta^7). \tag{29}$$

Comparison of one, two and three terms of this series with the numerically-obtained values are shown in Fig. 1 and above in Table 1.

It is clear that even two terms in the series provides extremely accurate approximations of the exact solutions even though the series progresses in terms of the square root of the logarithm of $-\epsilon$ and logarithms of that, and would therefore be expected to converge exceptionally slowly as Rb decreases towards zero. But here we see that there is an error in the two-term series of less than 1% when $\epsilon = 10^{-2}$, and this reduces to 0.1% when $\epsilon = 10^{-5}$. These percentage errors reduce to 0.1% and 0.002%, respectively, when taking four terms.

It remains now to substitute Eq. (29) into Eq. (17) to find the small–ϵ behaviour of $F(\mathrm{Rb})$, which is also shown in Fig. 2. Therefore we find that,

$$F(\mathrm{Rb}) = 1 - e^{-\eta^2} = 1 - \frac{\epsilon\sqrt{\pi}}{\delta}\left[1 + \frac{\mathcal{D}+1}{2}\delta^2 - \frac{\mathcal{D}^2 + 4\mathcal{D} + 6}{8}\delta^4 + O(\mathcal{D}^3\delta^6)\right]. \tag{30}$$

Consideration of the behaviour of the second term in this series shows that the slope of the curve is infinite at $\mathrm{Rb} = 0$, but that it is a very weak singularity indeed.

References

[1] H.A. Barnes, The yield stress – a review or '$\pi\alpha\nu\tau\alpha\ \rho\epsilon\iota$' – everything flows?, J Non-Newtonian Fluid Mech. 81 (1999) 133–178.
[2] S.W. Jeong, Determining the viscosity and yield surface of marine sediments using modified Bingham models, Geosci. J. 17 (3) (2013) 241–247.
[3] A. Maßmeyer, Thermal instabilities in a yield-stress fluid: from the laboratory to the planetary scale (PhD thesis), Université Paris Sud., 2013.
[4] A.V. Shenoy, Non-Newtonian fluid heat transfer, Adv. Heat Transfer 24 (1991) 102–190.
[5] T. Sochi, M.J. Blunt, Pore-scale network modeling of Ellis and Herschel–Bulkley fluids, J. Petrol. Sci. Eng. 60 (2008) 105–124.
[6] M.A. Hassan, M. Pathak, M.K. Khan, Natural convection of viscoplastic fluids in a square enclosure, Trans. A.S.M.E., J. Heat Transfer 135 (2013) 122501.
[7] O. Turan, N. Chakraborty, R.J. Poole, Laminar natural convection of Bingham fluids in a square enclosure with differentially heated side walls, J. Non-Newtonian Fluid Mech. 165 (2010) 901–913.
[8] O. Turan, R.J. Poole, N. Chakraborty, Aspect ratio effects in laminar natural convection of Bingham fluids in rectangular enclosures with differentially heated side walls, J. Non-Newtonian Fluid Mech. 166 (2011) 208–230.
[9] O. Turan, R.J. Poole, N. Chakraborty, Influences of boundary conditions on laminar natural convection of Bingham fluids in rectangular enclosures with differentially heated side walls, Heat Transfer Eng. 35 (9) (2014) 822–849.
[10] A. Vikhansky, On the onset of natural convection of Bingham liquid in rectangular enclosures, J. Non-Newtonian Fluid Mech. 165 (2010) 1713–1716.
[11] D. Vola, L. Boscardin, J.C. Latché, Laminar unsteady flows of Bingham fluids: a numerical strategy and some benchmark results, J. Comput. Phys. 187 (2003) 441–456.
[12] W.J. Yang, H.C. Yeh, Free convective flow of Bingham plastic between two vertical plates, Trans. A.S.M.E., J. Heat Transfer 87 (2) (1965) 319–320.

[13] Y. Bayazitoglu, P.R. Paslay, P. Cernocky, Laminar Bingham fluid flow between vertical parallel plates, Int. J. Therm. Sci. 46 (2007). pp. 349–335.
[14] I. Karimfazli, I.A. Frigaard, Natural convection flows of a Bingham fluid in a long vertical channel, J. Non-Newtonian Fluid Mech. 201 (2013) 39–55.
[15] N. Patel, D.B. Ingham, Analytic solutions for the mixed convection flow of non-Newtonian fluids in parallel plate ducts, Int. Commun. Heat Mass Transfer 21 (1) (1994) 75–84.
[16] A. Barletta, E. Magyari, Buoyant Couette–Bingham flow between vertical parallel plates, Int. J. Therm. Sci. 47 (2008) 811–819.
[17] J. Kleppe, W.J. Marner, Transient free convection in a Bingham plastic on a vertical flat plate, Trans. A.S.M.E., J. Heat Transfer 94 (4) (1972) 371–376.
[18] S. Ostrach, An analysis of laminar free-convection flow and heat transfer about a flat plate parallel to the direction of the generating body force, NACA report-1111, 1953.
[19] D.A.S. Rees, Convection of a Bingham fluid in a porous medium, in: K.Vafai (Ed.), Handbook of Porous Media, vol. III, Taylor and Francis, in press.
[20] H. Pascal, Nonsteady flow through porous media in the presence of a threshold gradient, Acta Mech. 39 (1981) 207–224.
[21] E. Buckingham, On plastic flow through capillary tubes, Proc. Am. Soc. Test. Mater. 21 (1921) 1154–1156.
[22] P.R.S. Mendes, M.F. Naccache, C.V.M. Braga, A.O. Nieckele, F.S. Ribeiro, Flows of Bingham materials through ideal porous media: an experimental and theoretical study, J. Brazil. Soc. Mech. Eng. 24 (1) (2002) 40–45.
[23] M.T. Balhoff, K.E. Thompson, Modeling the steady flow of yield-stress fluids in packed beds, Am. Inst. Chem. Eng. J. 50 (2004) 3034–3048.
[24] H. Liu, J. Wang, Y. Xie, D. Ma, X. Shi, Flow characteristics of heavy oil through porous media. Energy sources Part A, Recovery Util. Environ. Effects 34 (2012) 347–359.
[25] D.A.S. Rees, Vortex instability from a near-vertical heated surface in a porous medium I. Linear theory, Proc. Roy. Soc. A457 (2001) 1721–1734.
[26] A. Selim, D.A.S. Rees, The stability of a developing thermal front in a porous medium I. Linear theory, J. Porous Media 10 (2007) 1–16.